

CHAPTER 16

Wide-Angle Water Wave Models Using Fourier Method

Robert A. Dalrymple,¹ Member, ASCE
Kyung Duck Suh,² Associate Member, ASCE

Abstract: Two Fourier models for the propagation of surface waves are reported, which are theoretically valid for angles of propagation up to $\pm 90^\circ$ with respect to normal incidence. This is a great improvement in comparison with the present parabolic models. The first model is based on the assumption of straight and parallel depth contours, and the second one is the extension to the case of irregular bathymetry.

1 Introduction

The parabolic equation method has proven to be a convenient and rapid method for modelling the propagation of surface waves over water of varying depths, including such important phenomena as refraction and diffraction, e.g. Radder (1979), Booij (1981), Kirby & Dalrymple (1983), Liu & Tsay (1984). The small-angle approximation of this method, however, leads to errors if the wave direction deviates largely from the assumed propagation direction like the waves diffracted behind a breakwater, for example.

Very recently Dalrymple & Kirby (1988) developed a wave propagation model valid for angles of propagation up to 90° with respect to the assumed propagation direction (positive x direction in this paper), based on the assumption that the depth contours are straight and parallel in the y direction. This model was extended to the case of irregular bathymetry by Dalrymple *et al* (1988). In Dalrymple & Kirby, the incident wave train at $x = 0$ is decomposed into directional modes, or an angular spectrum, by taking the Fourier transform of the wave train in the y direction, and each directional mode propagates in the x direction only undergoing refraction and shoaling. In Dalrymple *et al*, however, bottom irregularities are shown to interact with nonzero directional modes and to force the evolution of other directional modes, even if they are initially of zero magnitude. In this paper, these two models are briefly summarized and various examples are presented.

2 Linear Fourier model – Straight and parallel contours

The mild-slope equation developed by Birkhoff (1972) can be written, on a beach with straight and parallel (in the y direction) depth contours, as

$$(CC_g\Phi_x)_x + CC_g\Phi_{yy} + k^2CC_g\Phi = 0 \quad (1)$$

¹Prof., Dept. of Civ. Engrg., Univ. of Delaware, Newark, DE 19716.

²Res. Asst., Dept. of Civ. Engrg., Univ. of Delaware, Newark, DE 19716.

where C and C_g are the phase and group velocities, respectively, k is the wavenumber, and $\Phi(x, y)$ is the free surface elevation obtained by dropping the harmonic time dependence. The Fourier transform of the above equation in the y direction leads to the decomposition of the potential into directional modes

$$(CC_g \hat{\Phi}_x)_x + (k^2 - \lambda^2)CC_g \hat{\Phi} = 0 \tag{2}$$

where the caret denotes a variable in the Fourier space and λ is the continuous Fourier parameter.

Splitting the potential into the forward propagating and backscattered potentials and neglecting the assumed small backscattered wave (see Dalrymple & Kirby (1988) for details), the propagation model for the forward propagating wave (denoted by the superscript +) is obtained as

$$\hat{\Phi}_x^+ = i\sqrt{k^2 - \lambda^2} \hat{\Phi}^+ - \frac{[CC_g \sqrt{k^2 - \lambda^2}]_x}{2CC_g \sqrt{k^2 - \lambda^2}} \hat{\Phi}^+. \tag{3}$$

This equation can be solved analytically to give the solution

$$\hat{\Phi}^+(x, \lambda) = \hat{\Phi}^+(0, \lambda) \left[\frac{(CC_g)_o \sqrt{k_o^2 - \lambda^2}}{CC_g \sqrt{k^2 - \lambda^2}} \right]^{1/2} e^{i \int \sqrt{k^2 - \lambda^2} dx} \tag{4}$$

where the subscript o indicates initial conditions at $x = 0$. The bracketed term contains the shoaling and refraction coefficients associated with gradual water depth changes (e.g. Dean & Dalrymple (1984)).

Under the assumption that the model domain is laterally periodic, the problem can be approximated in the discrete Fourier space. The domain is discretized in the y direction by N equidistant points, with spacing $\Delta y = \ell / (N - 1)$ where ℓ is the width of the domain. The velocity potential $\Phi^+(x, y)$, numerically defined only on these points, can be transformed into discrete Fourier modes by

$$\hat{\Phi}^+(x, n) = \frac{1}{N} \sum_{j=0}^{N-1} \Phi^+(x, j\Delta y) e^{-in\lambda j\Delta y}, \quad n = 0, \pm 1, \dots, \pm \left(\frac{N}{2} - 1\right), -\frac{N}{2}. \tag{5}$$

The inversion formula is

$$\Phi^+(x, j\Delta y) = \sum_n \hat{\Phi}^+(x, n) e^{in\lambda j\Delta y}, \quad j = 0, 1, \dots, (N - 1) \tag{6}$$

where

$$\lambda = \frac{2\pi}{N\Delta y} \tag{7}$$

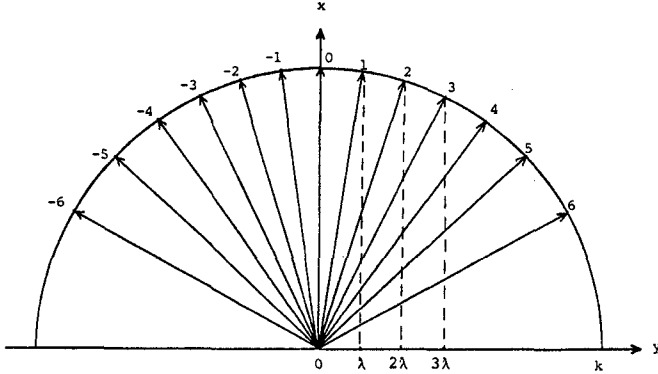


Figure 1: Diagram of the Fourier decomposition of the wave field on a row with an angular spectrum (with lateral wavenumbers, $n\lambda$, $n = 0, \pm 1, \pm 2, \dots$).

which is different from the continuous Fourier parameter λ used before. Subsequently, λ is defined by (7) if it is used in the discrete Fourier space. These transforms can be performed efficiently by using a fast Fourier transform (FFT for short) with $N = 2^p$ where p is a positive integer. Now the equation (4) can be expressed, in the discrete Fourier space, as

$$\hat{\Phi}^+(x, n) = \hat{\Phi}^+(0, n) \left[\frac{(CC_g)_o \sqrt{k_o^2 - (n\lambda)^2}}{CC_g \sqrt{k^2 - (n\lambda)^2}} \right]^{1/2} e^{i \int \sqrt{k^2 - (n\lambda)^2} dx}, \tag{8}$$

$$n = 0, \pm 1, \pm 2, \dots, \pm \left(\frac{N}{2} - 1 \right), -\frac{N}{2}.$$

Here $\hat{\Phi}^+(x, n)$ denotes the directional modes of the wave field on a row, each has the direction depicted in Fig. 1. As $n\lambda$ exceeds k in magnitude, $\sqrt{k^2 - (n\lambda)^2}$, the wavenumber in the x direction, becomes imaginary, indicating evanescent modes which decay exponentially in the propagation direction. Usually the evanescent modes have negligible amplitude with sufficiently large N , so only the progressive modes are carried in the computation.

2.1 Periodic gaps in breakwaters

For periodic gaps of width $2a$ in breakwaters, the initial condition is given by the Kirchoff condition on Φ_x^\pm along the breakwater, i.e.

$$\Phi_x^+(0, y) = \begin{cases} e^{i\lambda_o y}, & |y| < a \\ 0, & |y| > a \end{cases} \tag{9}$$

where λ_o is the projection of the wavenumber in the y direction at $x = 0$, that is, $\lambda_o = k_o \sin \theta_o$, where θ_o is the incident wave angle, and the origin of the coordinates is located at

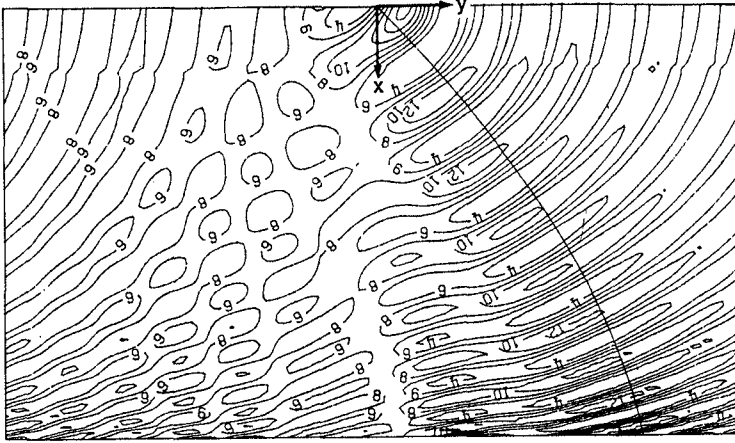


Figure 2: Instantaneous wave field behind periodic breakwater gaps on a sloping beach. The line denotes a wave ray, emanating from the center of one of the gaps. Depicted area is $405.75 \times 692.48 \text{ m}$. (reprinted with permission of Cambridge University Press)

the center of one of the gaps. $\hat{\Phi}_x^+(0, n)$ is obtained by an FFT of (9), and then $\hat{\Phi}^+(0, n)$ is computed by

$$\hat{\Phi}_x^+(0, n) = i\sqrt{k_o^2 - (n\lambda)^2} \hat{\Phi}^+(0, n) \tag{10}$$

which is the reduced form of (3) on constant depth. Finally $\Phi^+(0, y)$ is obtained by an inverse FFT of $\hat{\Phi}^+(0, n)$.

The breakwater gap shown in Fig. 2 is backed by a plane sloping beach with a slope $h_x = 0.0308k_o h_o$ where $h_o = 10 \text{ m}$ is the water depth at the location of breakwater. The gap has a width of 100 m . The incident wave field has a 9 sec wave period and a 45° angle of incidence. $N = 128$ and $\Delta x = \Delta y = 5 \text{ m}$. In Fig. 2, the instantaneous wave field on the sloping beach is shown. The influence of wave refraction is clear with the maximum of the diffraction pattern turning towards the shoreline normal. The influence of the periodic boundary conditions is also apparent as the waves from the upwave gap have intruded into the figure, yielding a short-crested sea state near the middle of the figure. The wave ray shown in the figure was determined independently using the method outlined in Mei (1983). The diffracting wave train follows the wave ray very well.

2.2 Intersecting waves past a breakwater

The specification of the incident wave field can be quite general. As a simple example, two synchronous wave trains of 9 sec period are assumed to be incident on a breakwater (386 m in length, lying on the y axis) at $\pm 30^\circ$ to each side of the x axis, creating a short-crested sea state in the absence of the breakwater, as shown in Fig. 3. Behind the breakwater, centered in the middle of the y axis, the two shadow zones cast by the two wave trains

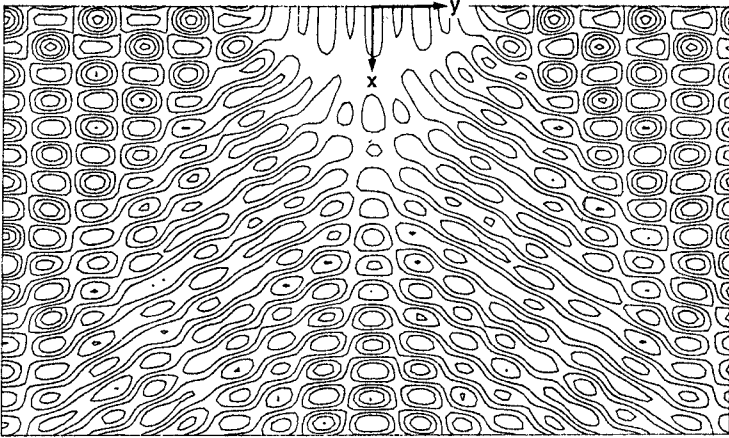


Figure 3: Instantaneous wave field behind an offshore breakwater created by two intersecting wave trains. The breakwater length is 386 m and the displayed area is 1016 m wide. (reprinted with permission of Cambridge University Press)

result in a long-crested sea state in these zones, as only one of the wave trains is blocked by the breakwater.

Extension to a truly directional sea state composed of many frequencies is straightforward. It is a matter of superposing the requisite number of wave trains with different frequencies and appropriate random phases, since for each frequency the evolution of the directional spectrum is computed in the present model.

3 Nonlinear Fourier model on irregular bathymetry

The governing equation is again taken to be the mild-slope equation

$$\nabla \cdot (CC_g \nabla \Phi) + k^2 CC_g \Phi = 0. \quad (11)$$

The wavenumber k is related to the wave angular frequency ω and the local water depth h by the linear dispersion relationship

$$\omega^2 = gk \tanh kh \quad (12)$$

where g is gravity. This relation is modified later to incorporate nonlinearity in the model.

Using the definitions of $p(x, y) = CC_g$ and $\phi = \sqrt{p} \Phi$ as in Radder (1979), the mild-slope equation becomes an Helmholtz equation

$$\nabla^2 \phi + k_c^2 \phi = 0 \quad (13)$$

where

$$k_c^2 = k^2 - \frac{\nabla^2 \sqrt{p}}{\sqrt{p}}. \tag{14}$$

For the convenience of later splitting of the solution, we define a laterally averaged wavenumber, \bar{k} , as

$$\bar{k}^2 = \frac{1}{\ell} \int_0^\ell k_c^2 dy \tag{15}$$

so that

$$k_c^2 = \bar{k}^2 (1 - \nu^2) \tag{16}$$

where

$$\nu^2 = 1 - \frac{k_c^2}{\bar{k}^2} \tag{17}$$

whose magnitude is usually much smaller than unity if the topography does not deviate drastically from straight and parallel contours. Note that \bar{k}^2 is a function of x only and the variability of depth in the y direction is contained in $\nu^2(x, y)$. Substituting (16) into (13) gives

$$\nabla^2 \phi + \bar{k}^2 \phi - \bar{k}^2 \nu^2 \phi = 0. \tag{18}$$

The Fourier transform of (18) in the y direction leads to the equations for directional modes

$$\hat{\phi}_{xx} + (\bar{k}^2 - \lambda^2) \hat{\phi} - \bar{k}^2 F(\nu^2 \phi) = 0. \tag{19}$$

Note that the Fourier transform of $(\nu^2 \phi)$ involves ϕ in the real space. Again splitting the potential and neglecting the backscattered wave, the propagation model for the forward propagating wave is obtained as

$$\hat{\phi}_x^\pm = i\sqrt{\bar{k}^2 - \lambda^2} \hat{\phi}^\pm - \frac{[\sqrt{\bar{k}^2 - \lambda^2}]_x}{2\sqrt{\bar{k}^2 - \lambda^2}} \hat{\phi}^\pm - \frac{i\bar{k}^2 F(\nu^2 \phi^\pm)}{2\sqrt{\bar{k}^2 - \lambda^2}}. \tag{20}$$

The second term on the right side represents the shoaling/refraction of each wave mode on the laterally averaged depths. The $F(\nu^2 \phi^\pm)$ term represents the interaction between

surface wave and the lateral bottom variation, which will be examined in detail later in this section. For straight and parallel bottom contours, this term vanishes and the above equation reduces to (3).

In the discrete Fourier space, (20) can be approximated as

$$\hat{\phi}_x^+ = i\sqrt{k^2 - (n\lambda)^2} \hat{\phi}^+ - \frac{[\sqrt{k^2 - (n\lambda)^2}]_x}{2\sqrt{k^2 - (n\lambda)^2}} \hat{\phi}^+ - \frac{i\bar{k}^2 F_n(\nu^2 \phi^+)}{2\sqrt{k^2 - (n\lambda)^2}}, \quad (21)$$

$$n = 0, \pm 1, \pm 2, \dots, \pm\left(\frac{N}{2} - 1\right), -\frac{N}{2}$$

associated with the discrete Fourier transforms (5) and (6). F_n denotes the n^{th} Fourier component. The above equation represents N first-order ordinary differential equations in x , which are solved by a fourth-order Runge-Kutta method. The details of finite differencing and stability analysis of the numerical method are referred to Dalrymple *et al* (1988). The numerical procedure involves calculating the Fourier modes by marching along the x direction. However, $F_n(\nu^2 \phi^+)$ in the last term in (21) should be calculated in the real domain, so, at each step, recourse to the real domain by the inverse FFT is needed.

The Fourier model (21) is linear since it is based on the linear mild-slope equation (11). In order to incorporate nonlinearity in the model, an empirical nonlinear dispersion relation proposed by Kirby & Dalrymple (1986) is used, which approximates the wavenumber for a solitary wave in shallow water and, in deep water, provides the wavenumber corresponding to the Stokes third-order theory, given by

$$\omega^2 = gk[1 + f_1(ka)^2 D] \tanh[kh + f_2(ka)] \quad (22)$$

where a is the local wave amplitude and

$$f_1(kh) = \tanh^5 kh, \quad (23)$$

$$f_2(kh) = \left[\frac{kh}{\sinh kh} \right]^4, \quad (24)$$

$$D = \frac{\cosh 4kh + 8 - 2 \tanh^2 kh}{8 \sinh^4 kh}. \quad (25)$$

The calculation of the wavenumber k using (22) needs iteration because of the dependence of the wavenumber on wave height. Thus, first we perform the computation with the wavenumber given by the linear dispersion relation (12). Using the calculated wave height, then, the wavenumber is corrected by the nonlinear dispersion relation (22). This procedure is repeated until convergence is achieved.

3.1 Interaction between surface wave modes and the bottom variation

The term $F_n(\nu^2 \phi^+)$ in (21) represents the interaction between the directional wave modes and the lateral bottom variation, which can force the evolution of the various directional

modes, even if they are initially of zero magnitude. In order to examine this mechanism, we express $F_n(\nu^2\phi^+)$, in terms of periodic convolution, as

$$F_n(\nu^2\phi^+) = \frac{1}{N} \sum_{m=0}^{N-1} \hat{\nu}^2(x, m\lambda) \hat{\phi}^+(x, (n-m)\lambda) \quad (26)$$

where $\hat{\nu}^2(x, m\lambda)$, $m = 0$ to $N - 1$, is the discrete Fourier series obtained by the Fourier transform of $\nu^2(x, y)$ in the y direction. This equation states that the m^{th} bottom mode $\hat{\nu}^2(x, m\lambda)$ triggers the $(n - m)^{th}$ wave mode to evolve the n^{th} wave mode.

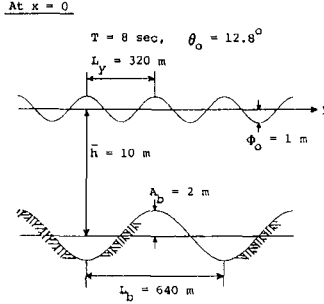


Figure 4: Bottom geometry and the initial condition of the wave field for the example of wave propagation over a bathymetry consisting of laterally periodic ridges and troughs.

In order to illustrate this more explicitly, we have applied the model to a monochromatic wave train travelling over a bed whose depth is constant in the x direction but varies sinusoidally in the y direction, creating transverse bottom ridges. These ridges begin at $x = 0$. In this particular example, the second term on the right side in (21) vanishes. The mean water depth is 10 m and the wavelength and amplitude of the bed are 640 m and 2 m, respectively, as shown in Fig. 4. At $x = 0$, a plane wave of 8 sec period and 1 m amplitude enters the domain at an incident angle of 12.8°. We have taken $\Delta x = 5$ m and $\Delta y = 10$ m to make a grid of 500 × 128 rows over 2,500 × 1,280 m model area, so that the wave mode at $x = 0$, $\hat{\phi}^+(0, n\lambda)$, is nonzero for $n = 4$ and zero for all other modes, while the bottom mode $\hat{\nu}^2(x, m\lambda)$ are appreciable for $m = 2, 4, 6, (N - 6), (N - 4), (N - 2)$ and are negligibly small for all other modes as shown in Fig. 5. At the first step, these bottom modes interact with $\hat{\phi}^+(0, 4\lambda)$ to generate the wave modes of $n = 6, 8, 10, -2, 0, 2$, respectively, which were initially of zero magnitude. Note that in an FFT, the following changes are made: $\hat{\nu}^2(x, (N - m)\lambda) = \hat{\nu}^2(x, -m\lambda)$. The mechanism for the subsequent generation of new directional modes is very complicated. Note that only the even-number modes are generated in this particular example.

Figs. 6 (a)–(d) show the amplitude spectra of the progressive modes at different sections. The wave field at $x = 0$ (Fig. 6 (a)) is described by single wave mode, $\hat{\phi}^+(0, 4\lambda)$, which is propagating at 12.8° to the x axis. The generation of new modes near the initial condition is shown in Figs. 6 (b)–(c), and the broad spectrum at $x = 2,500$ m is shown in Fig. 6 (d). Again observe that the odd-number modes are never generated.

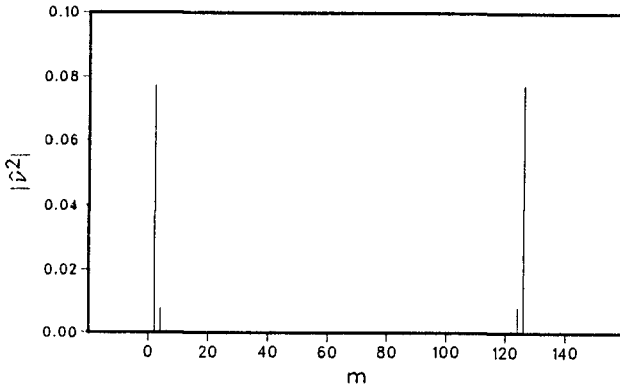


Figure 5: Amplitude spectrum of the bottom modes $\hat{\nu}^2(x, m\lambda)$ for the periodic bathymetry shown in Fig. 4. Note that $\hat{\nu}^2(x, m\lambda)$ is different from the depth mode $\hat{h}(x, m\lambda)$ which gives nonzero values for $m = 2$ and $N - 2$ and zero for all other values of m .

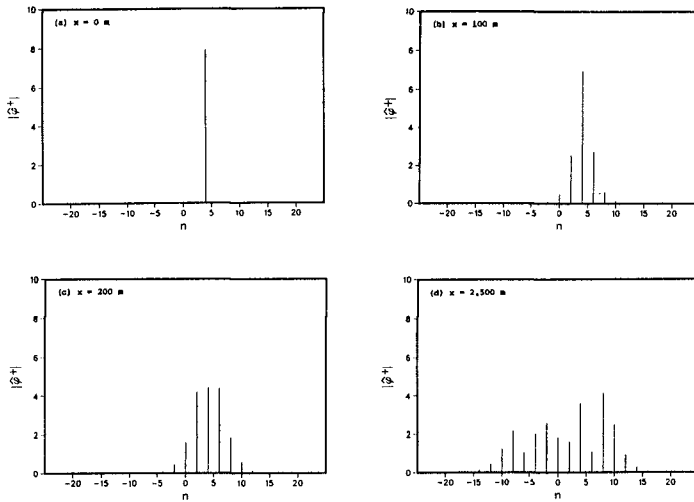


Figure 6: Evolution of the amplitude spectra of the progressive modes at different sections.

Another interesting result in this example is the wave trapping over the ridge as shown in Fig. 7, which is the contour map of the instantaneous free surface elevation at intervals of 0.5 m. The waves passing over the central ridge are focused near $x = 700\text{ m}$, $y = 720\text{ m}$ and turn back to the left. Mei (1983) has discussed this problem based on ray theory. Some of the rays determined by the Mei's method are drawn in Fig. 7. The rays 1, 2 and 8, counting from the left, travel over the wavy bed without being trapped. The rays 3 to 7,

however, are trapped. For these rays computation was stopped at the turning points, where the ray model blows up, but the extrapolation of these rays can explain the wave trapping phenomenon over the ridge in this example.

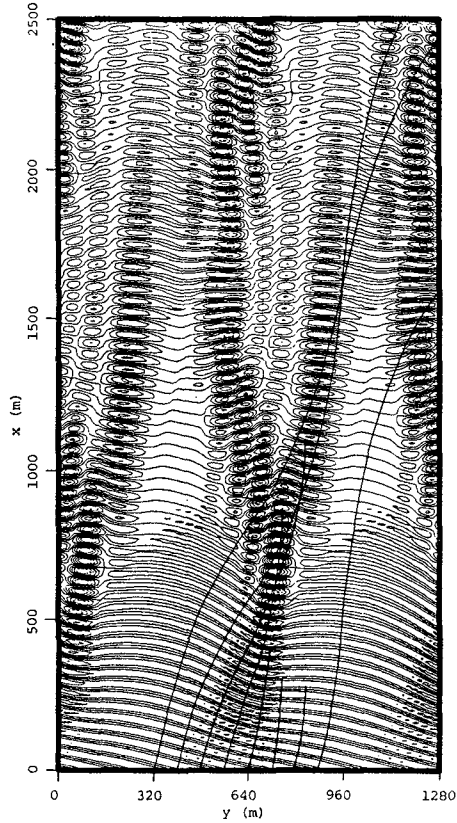


Figure 7: Instantaneous wave field over periodic ridges and troughs. The lines denote wave rays emanating from $x = 0$ at 12.8° angle of incidence at intervals of 80 m .

3.2 Wave focusing behind a circular shoal

For the purpose of testing the model for the prediction of wave deformation on an irregular bathymetry, we have chosen the experiment reported by Ito & Tanimoto (1972).

The experimental bathymetry consists of a circular shoal resting on a flat bottom $h_1 = 0.15\text{ m}$ as shown in Fig. 8. The water depths in the shoal region are described by

$$h = h_2 + 0.15625[(x - 1.2)^2 + (y - 1.2)^2] \quad (27)$$

where $h_2 = 0.05 \text{ m}$ is the depth at the shoal crest. A monochromatic wave train with the wave height 1.04 cm and the wave period 0.511 sec enters the domain at $\theta_o = 0^\circ$.

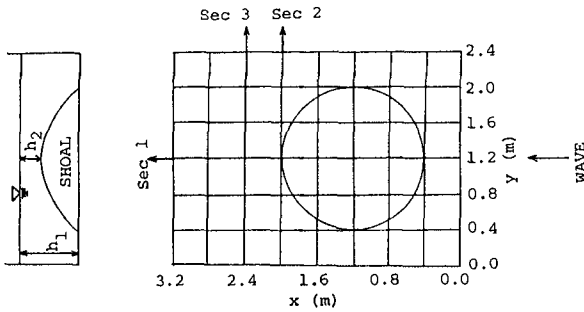


Figure 8: Geometry of the computational domain for the experiment by Ito & Tanimoto (1972).

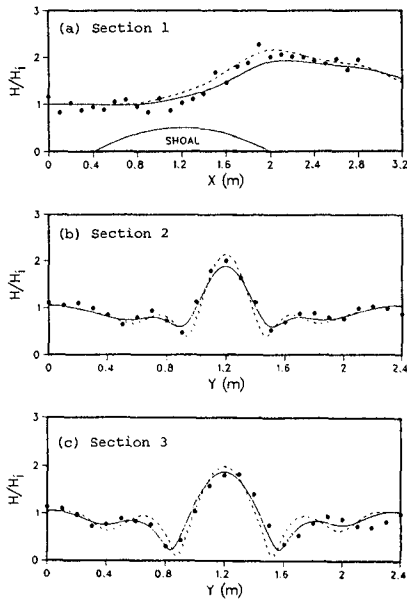


Figure 9: Comparison of the model results against the experimental data by Ito & Tanimoto (1972) in terms of normalized wave height with respect to incident wave height. ● = Experiment, - - - = Linear model, — = Nonlinear model.

For the three different sections indicated in Fig. 8, data from the experiment of Ito & Tanimoto are available. Comparison with the model results along these sections are shown in Figs. 9 (a)–(c) in terms of normalized wave height with respect to the incident wave height. In each figure, linear and nonlinear model results are indicated by dashed and solid lines, respectively, while black dots indicate measured data points. Nonlinear effects reduce the wave heights along the centerline of wave focusing and broaden the region of focused wave so that the diffraction fringes are displaced away from the centerline. Along the centerline (Fig. 9 (a)), data fall between the predictions of the two models, with the nonlinear model slightly underpredicting the data. On section 2 where the cusped caustic is fully developed, again it is difficult to judge which model predicts the data better. However, on section 3 where the wave has passed through the caustic cusp, the nonlinear model predictions and the data points are in much better agreement than the linear model.

Through the above example we have verified that our model is a reasonably good predictor of the wave field development on an irregular bathymetry where the effects of refraction, diffraction and nonlinearity are equally significant. However, that example is not sufficient for showing the ability of the model for a large angle of incidence. The next example we have chosen for this purpose is for the same wave and bottom geometry as those in the above example but different angle of incidence. Due to the axisymmetry of the circular shoal, the wave focusing pattern behind the shoal should be independent of the angle of incidence, if the model predicts it 'correctly'.

The contours of wave height normalized with respect to the incident wave height are shown in Figs. 10 (a) and (b) for $\theta_o = 0^\circ$ and $\theta_o = 45^\circ$, respectively. The right half of the domain in the case of $\theta_o = 45^\circ$ is the extension of the flat bottom. The results of a linear parabolic model are also shown in Fig. 10 (a) as dotted lines for $\theta_o = 0^\circ$ and in Fig. 10 (c) for $\theta_o = 45^\circ$. The difference between the present model and the parabolic one is not significant for $\theta_o = 0^\circ$ even though the entire wave focusing pattern in the parabolic model is shifted slightly backward compared with that in the present model. For $\theta_o = 45^\circ$, however, the parabolic model gives large distortion of the wave focusing pattern. Especially the center line of wave focusing rotates by about 12.5° towards the positive x direction. For the present model, some images of the shoal appear periodically in the y direction and the upper left corner is contaminated by the effects of the upwave shoal. Over the shoal, the asymmetric distortion to the focusing pattern at $\theta_o = 45^\circ$ is apparent. However, the overall wave focusing pattern behind the shoal at $\theta_o = 45^\circ$ is very similar to that at $\theta_o = 0^\circ$, showing that the model works reasonably well for a large angle of incidence.

The height of the shoal in the above example is $2/3$ of the water depth on the flat bottom, indicating an unreasonably high shoal considering the normal situation in real cases. Dalrymple *et al* (1988) have tested the model for shallower shoals and showed that the bigger the shoal height, the bigger the asymmetric distortion to the focusing pattern for the same angle of incidence. They also have presented a simple theoretical analysis regarding the accuracy of the model in terms of lateral depth variation and wave propagation angle, concluding that in order for the present model to be accurate for a large angle of incidence, the lateral depth variation should be small.

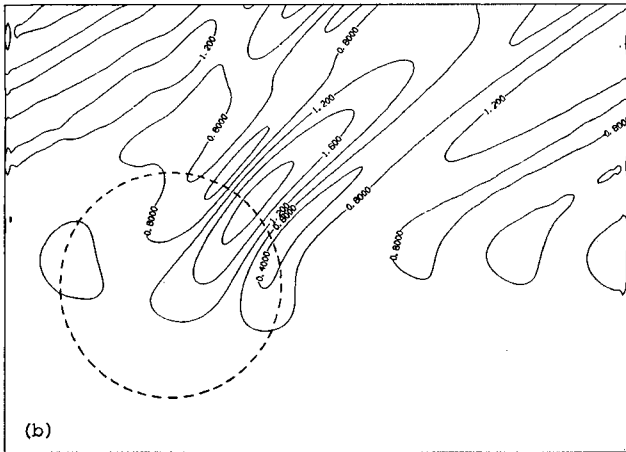
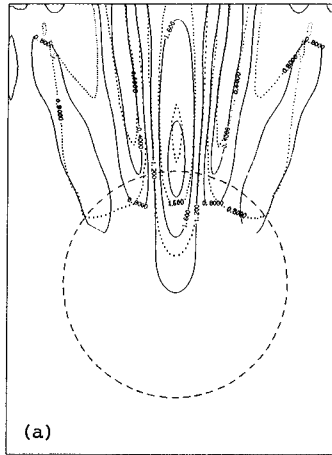


Figure 10: For caption see next page.

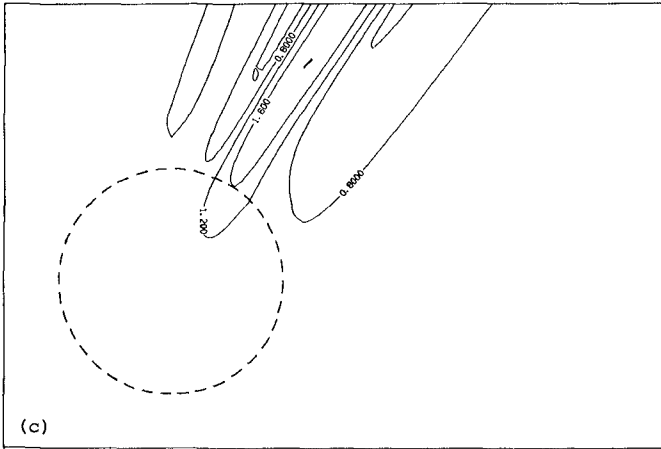


Figure 10: Wave focusing pattern behind the circular shoal used in the experiment by Ito & Tanimoto (1972). Contours indicate wave height normalized with respect to incident wave height. (a) $\theta_o = 0^\circ$ (— = Present model, = Parabolic model), (b) $\theta_o = 45^\circ$ (Present model), (c) $\theta_o = 45^\circ$ (Parabolic model).

4 Conclusion and discussion

Two wide-angle water wave propagation models using the spectral Fourier method have been reported, one for straight and parallel depth contours and the other for irregular bathymetry. In both of the models, the wave field at the initial row ($x = 0$) is Fourier decomposed into directional modes and the evolution of each mode due to bottom variation is calculated by marching along the x direction; finally, the real wave field is recovered by taking the inverse Fourier transform in the y direction.

All the examples presented are for a monochromatic wave train or two intersecting waves. As demonstrated in the example of two intersecting waves past a breakwater, a directional wave with single frequency can be modelled easily by the present models. If the steady state is assumed so that the interaction among the waves with different frequencies is neglected, the extension of the models to the random directional wave field can be made by superposing the requisite number of waves with different frequencies, with appropriate phases.

Nonlinearity was included in the model by correcting the wavenumbers iteratively using the nonlinear dispersion relationship, (22). Wave-current interaction also could be included by using the following dispersion relationship

$$\sigma = \omega + \vec{k} \cdot \vec{U} \quad (28)$$

where $\sigma = 2\pi/T$ is newly defined as the angular frequency, ω is given by (22), and \vec{U} is the depth-mean current vector which is assumed to be known.

Acknowledgement

This work is partly a result of research sponsored by NOAA Office of Sea Grant, Department of Commerce, under Grant No. NA86AADSG040. The U.S. Government is authorized to produce and distribute reprints for governmental purposes, notwithstanding any copyright notation that may appear herein.

References

- Berkhoff, J.C.W. 1972. Computation of combined refraction-diffraction. *Proc. 13th Int. Conf. Coastal Eng.*, ASCE, Vancouver. 471-490.
- Booij, N. 1981. Gravity waves on water with non-uniform depth and current. *Rep. 81-1*, Dept. of Civil Eng., Delft Univ. of Tech.
- Dalrymple, R.A. & Kirby, J.T. 1988. Models for very wide-angle water waves and wave diffraction. *J. Fluid Mech.* 192. 33-50.
- Dalrymple, R.A., Suh, K.D., Kirby, J.T. & Chae, J.W. 1988. Models for very wide-angle water waves and wave diffraction. Part 2. Irregular bathymetry. *J. Fluid Mech.* (in review)
- Dean, R.G. & Dalrymple, R.A. 1984. *Water wave mechanics for engineers and scientists*. Englewood Cliffs: Prentice-Hall. 353pp.
- Ito, Y. & Tanimoto, K. 1972. A method of numerical analysis of wave propagation: Application to wave diffraction and refraction. *Proc. 13th Int. Conf. Coastal Eng.*, ASCE, Vancouver. 503-522.
- Kirby, J.T. & Dalrymple, R.A. 1983. A parabolic equation for the combined refraction-diffraction of Stokes waves by mildly varying topography. *J. Fluid Mech.* 136. 453-466.
- Kirby, J.T. & Dalrymple, R.A. 1986. An approximate model for nonlinear dispersion in monochromatic wave propagation models. *Coastal Eng.* 9. 545-561.
- Liu, P.L.-F. & Tsay, T.-K. 1984. Refraction-diffraction model for weakly nonlinear water waves. *J. Fluid Mech.* 141. 265-274.
- Mei, C.C. 1983. *The applied dynamics of ocean surface waves*. New York: Wiley-Interscience. 740pp.
- Radder, A.C. 1979. On the parabolic equation method for water-wave propagation. *J. Fluid Mech.* 95. 159-176.